A Discrete Element Method recast as a lowest-order discontinuous Galerkin method and applications to elasto-plastic solid dynamics

F. MARAZZATO[1,2,3], A. ERN[1,2], L. MONASSE[4] et K. SAB[5]

[1]Université Paris-Est, Cermics (ENPC), F-77455 Marne-la-Vallée cedex 2
email: {alexandre.ern, frederic.marazzato}@enpc.fr
[2]Inria, 2 rue Simone Iff, 75589 Paris, France
[3]CEA, DAM, DIF, F-91297 Arpajon, France
[4] Inria, Team COFFEE, Sophia Antipolis and Université Nice Sophia Antipolis, CNRS and Laboratoire J. A. Dieudonné, UMR 7351, 06108 Nice, France
email: laurent.monasse@inria.fr
[5] Université Paris-Est, Laboratoire Navier, ENPC, IFSTTAR, CNRS UMR 8205, 6 et 8 avenue Blaise Pascal, 77455 Marne-la-Vallée Cedex 2, France
email: karam.sab@enpc.fr

Résumé :

Nous proposons un nouveau schéma Elements Discrets utilisant des maillages polyédriques généraux. Ce schéma peut être réinterprété comme une méthode de Galerkin discontinue d'ordre minimal dont les paramètres sont ceux du modèle continu (module de Young et coefficient de Poisson). Ce schéma est également une généralisation de [1] permettant de faire des calculs élasto-plastiques. Le stencil a été étendu des voisins au sens des faces aux voisins des voisins. Le coût de calcul reste modéré car un schéma explicite est utilisé pour l'intégration temporelle et la matrice de masse est naturellement diagonale. La convergence du schéma peut être prouvée en utilisant le cadre des méthodes de discretisation de gradients. Des résultats numériques illustrent la robustesse et la versatilité du schéma proposé pour la dynamique des solides élasto-plastiques.

Abstract:

We propose a new discrete element method using general polyhedral meshes. The method can be understood as a lowest-order discontinuous Galerkin method parametrized by the continuous mechanical parameters (Young's modulus and Poisson's ratio). It can be viewed as a generalisation of [1] allowing to compute elasto-plastic constitutive laws. The stencil has been extended from nearest neighbours (in the sense of faces) to second-nearest neighbours. The computational cost of this extension is moderate since an explicit time-stepping method is used with a naturally diagonal mass matrix. The convergence of the numerical scheme can be proved using the framework of Gradient discretization methods. Numerical examples illustrate the robustness and versatility of the proposed method for elasto-plastic solid dynamics.

Mots clefs : Discrete Element Methods, Fast Dynamics, Explicit Time-integration, discretization of PDEs

1 Introduction

Since their early use by Hoover et al (1974) in models for crystalline materials and Cundall & Strack (1979) in geotechnical problems, Discrete Element methods (DEM) have found a large field of applications in granular materials, soil and rock mechanics. DEM consist in representing a domain by small spherical particles interacting by means of forces and torques. A wide variety of models for the expression of these bonds has been developed in the literature depending on the material constitutive law. Computing the deformation of the domain then consists in computing the evolution of this particulate system. To the best of our knowledge, generalising the DEM approach to compute Cauchy continua still remains a challenge. As highlighted in [3], actual methods require fitting parameters through numerical experiments. Also, actual methods meet with difficulties when simulating a material with a Poisson ratio $\nu \geq 0.3$.

Following the DEM approach, with a view to compute macroscopic deformations, the code Mka3D, developed by CEA and presented in [1], has allowed the simulation of a three-dimensional linear elastic material without suffering from locking in the incompressible limit. The discretization of the domain is achieved through Voronoi polyhedral particles, instead of spherical particles, considered as rigid solids. The computation of forces and momenta uses geometric quantities like the distance and relative rotation between two neighbouring particles. Moreover, only macroscopic parameters like Young's modulus and Poisson's ratio are used in the computations. However, this method is not a discretization method of a weak formulation of a Cauchy continuum and thus its convergence can be studied only by numerical experiments.

The aim of the present work is to introduce a lowest-order discontinuous Galerkin method using general polyhedral meshes with an extended stencil, in the spirit of [4], and that generalises the approach of [1] to elasto-plastic computations. Our method is derived from a natural discretization of dynamic elasto-plasticity written in weak form. We use piecewise constant gradient and displacement reconstructions on cells. Convergence can be studied using the framework of Gradient discretization methods [2]. Volumetric unknowns are also added to compute plastic strains. In addition, the coupling with an explicit Leapfrog integration to compute the time-evolution is presented.

This paper is organised as follows. The next section is a quick recall of the strong and weak form of the equations of dynamic elasto-plasticity in a Cauchy continuum. The third section presents the discretization of the weak formulation using the developed DEM and some numerical tests to verify the correct implementation of the space discretization. The final section presents a space-time discrete formulation and details the algorithm to compute dynamic elasto-plastic constitutive laws explicitly with a Störmer–Verlet time-integration.

2 Governing equations

The considered strain regime is restricted to small strains. The plastic constitutive law hinges on a Von Mises criterion with nonlinear isotropic hardening. The material is supposed to be homogeneous, isotropic and rate-independent. The presented formalism can be extended to the case of anisotropic, inhomogeneous, rate-dependent, anisothermal materials as well as finite strains.

2.1 Equations in strong form

Let $\Omega \subset \mathbb{R}^3$ be the domain of study. The problem is considered on the finite time interval $(0, T)$ where $T > 0$. Denote $\rho > 0$ the density of the material. Let $\partial\Omega = \partial\Omega_N \cup \partial\Omega_D$ be a partition of the boundary of Ω. The boundary $\partial\Omega_D$ has an imposed displacement $u_D(t)$, whereas an exterior stress $g(t)$ is imposed on $\partial\Omega_N$, and f is an imposed volumetric force. The fourth-order stiffness tensor is written $\mathbb{C}$. The equivalent stress is assumed to be a Von Mises stress: $\sigma_{eq} = \sqrt{\frac{3}{2}\mathrm{dev}(\sigma) : \mathrm{dev}(\sigma)}$, where dev is the deviatoric part of a second-order tensor and σ is the Cauchy stress tensor. Denote ε the linearised strain, ε_p the tensor remanent plastic deformation, p the scalar cumulated plastic deformation, σ_0 the initial yield stress and $\sigma_0 + R(p)$ the actual yield stress. The yield function of the stress is defined by:

$$\varphi(\sigma, p) = \sqrt{\frac{3}{2}}|\mathrm{dev}(\sigma)| - R(p) - \sigma_0. \tag{1}$$

The strong form of the dynamic elasto-plasticity equations with a Von Mises yield criterion in displacement form is to search for u and ε_p defined on $[0, T] \times \Omega$ such that:

$$\begin{cases} \mathrm{div}(\sigma) + f - \rho\ddot{u} = 0 \text{ in } \Omega, \\ \sigma = \mathbb{C} : (\varepsilon(u) - \varepsilon_p) \text{ in } \Omega, \\ u = u_D \text{ on } \partial\Omega_D, \\ \sigma \cdot n = g \text{ on } \partial\Omega_N, \\ \lambda\varphi(\sigma, p) = 0,\ \lambda \geq 0 \text{ and } \varphi(\sigma, p) \leq 0 \text{ in } \Omega, \\ \dot{\varepsilon}_p = \lambda\dfrac{\partial\varphi}{\partial\sigma} \text{ in } \Omega, \end{cases} \tag{2}$$

where $\lambda \geq 0$ is the Lagrange multiplier associated with the inequality constraint $\varphi(\sigma, p) \leq 0$. The initial conditions are given by:

$$\begin{cases} u(0) = u_0 \text{ in } \Omega, \\ \dot{u}(0) = v_0 \text{ in } \Omega. \end{cases} \tag{3}$$

2.2 Equations in weak form

The above elasto-plasticity equations can be recast as a variational inequality. The inequality comes from the yield criterion which discriminates between a purely elastic deformation and a plastic flow. The solution of equation (2) is searched as a couple $w(t) = (u(t), \varepsilon_p(t)) \in W$ evolving in time, where W is, at the same time, the space of solutions and test functions (up to the handling of Dirichlet conditions). Typically $W \subset H^1(\Omega)^3 \times \left(L^2(\Omega)\right)^{3\times 3}$ where $L^2(\Omega)$ is the space of square-integrable functions and $H^1(\Omega)$ a subspace of $L^2(\Omega)$ of functions whose weak gradient is also square-integrable.

The bilinear form corresponding to the work of internal stresses writes:

$$a(w(t), \tilde{w}) = \int_\Omega \left(\varepsilon\left(u(t)\right) - \varepsilon_p(t)\right) : \mathbb{C} : \varepsilon(\tilde{u}), \tag{4}$$

where $\tilde{w} = (\tilde{u}, \tilde{\varepsilon}_p) \in W$ is a test function. The bilinear form corresponding to the work of accelerations writes:

$$\langle \rho\ddot{u}(t), \tilde{u} \rangle_{W',W}\,, \tag{5}$$

where $\langle , \rangle_{W',W}$ is a duality pairing. The linear functional corresponding to the work of external loads writes:

$$\langle l(t), \tilde{w} \rangle_{W',W} = \int_\Omega f(t) \cdot \tilde{u} + \int_{\partial\Omega_N} g(t) \cdot \tilde{u}. \tag{6}$$

The dissipation associated with isotropic hardening is contained in a function $\omega_p \equiv \omega_p(p)$ which depends on the cumulated plastic strain p. The variation of the yield stress is then computed as $R(p) = -\frac{d\omega_p}{dp}$.

The variational formulation of Equation (2) writes: Find $w : (0,T) \longrightarrow W$ with $u(0) = u_0$, $\dot{u}(0) = v_0$ and $\varepsilon_p(0) = 0$, such that for almost every $t \in (0,T)$, $u(t) = u_D(t)$ on $\partial\Omega_D$ and:

$$\begin{cases} \langle \rho \ddot{u}(t), \tilde{u} \rangle_{W',W} + a(w(t), \tilde{w}) = \langle l(t), \tilde{w} \rangle_{W',W}, & \forall \tilde{w} \in W, \\ \varphi\left(\mathbb{C} : (\varepsilon(u(t)) - \varepsilon_p(t))\right) \leq 0, & \text{a.e in } \Omega. \end{cases} \tag{7}$$

3 Space discretization

In this section, the form of the discrete solution u_h is first described. The reconstruction of strains is then presented. Finally, the discrete problem is derived. The domain Ω is meshed with a mesh $\mathcal{T}_h$ of size h made of polyhedra with planar faces in 3D or polygons with straight edges in 2D.

Volumetric degrees of freedom (thereafter abbreviated dofs) for u_h are placed at the barycentre of every cell of $\mathcal{T}_h$. Boundary degrees of freedom for u_h are added at every vertex of the boundary facets. The discrete solution u_h is piecewise-constant with each piecewise component linked to a dof. Figure 1 illustrates the position of the dofs and the corresponding piecewise components of u_h. V_h denotes the space of discrete displacements u_h. In addition, a dof representing the internal variable is attached to each cell.

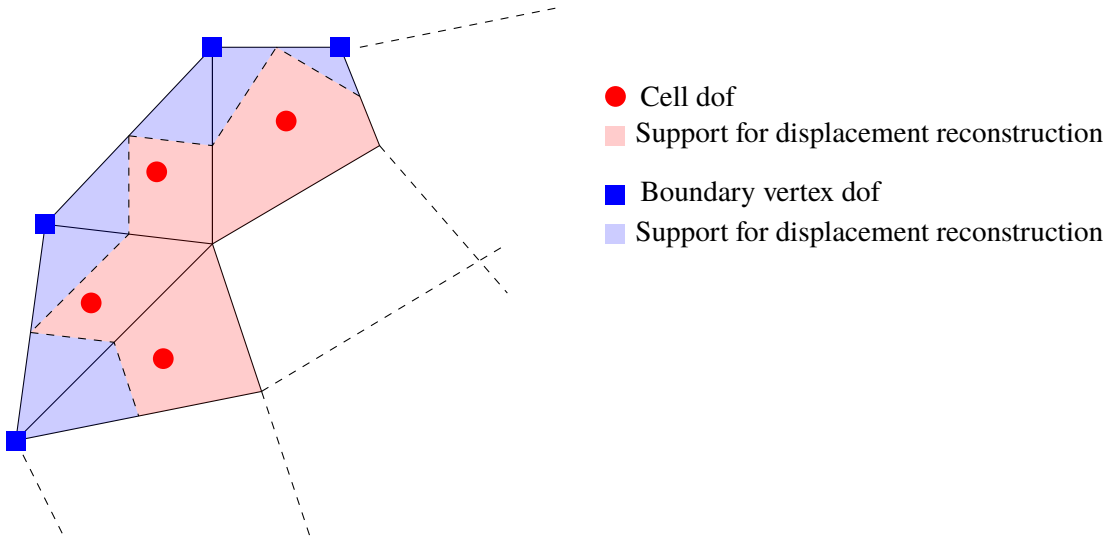

Figure 1: Degrees of freedom and discrete solution

3.1 Discretization of elastic forces

The proposed method hinges on piecewise-constant representations of the displacement field and at the same time, discrete gradients are reconstructed in order to compute the strains. The discrete gradients are reconstructed as piecewise-constant fields in Ω, i.e. constant in each cell. The method used to

reconstruct gradients is derived from the so called cell-centered Galerkin methods. These methods have been studied in [5, Sec. 2.2] and [4]. They consist in reconstructing a value on each facet using the values of neighbouring dofs. The reconstruction on interior facets is detailed first, then the reconstruction on boundary facets and finally the gradient reconstruction using the facet values is described.

3.1.1 Reconstruction on innner facets

The value in an inner facet is reconstructed using dofs attached to neighbouring cells. Boundary vertex dofs can be used as well. The number of dofs has to be one more than the dimension of the space, which means at least 4 in 3D and 3 in 2D, in such a way that the points associated with the dofs are the vertices of a tetrahedron that contains the facet barycentre. The displacement reconstructed on each interior facet is then a barycentric interpolation of the values of the above mentioned dofs. Figure 2 presents the reconstruction at the barycentre x_F of an interior facet F using neighbouring dofs located at x^i, x^j and x^k.

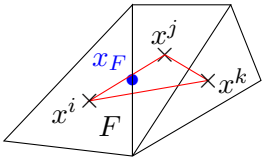

Figure 2: dofs associated with the interior facet F

Remark 1. *The two neighbouring cells of an interior facet F need not be used to reconstruct the value on F.*

Remark 2 (Interpolation VS Extrapolation)**.** *The value reconstructed at the facet barycentre is interpolated from well-chosen dofs as opposed to extrapolated from closest dofs. The boundary vertices dofs have been added so as to ensure that interpolating the value on every facet is always possible. Interpolation is preferred to extrapolation for dynamic computations for reasons explained in Section 4. However, if one desires to perform static or quasi-static computations, extrapolation using closest neighbours in the sense of facets is enough.*

3.1.2 Reconstruction on boundary facets

The value at the barycentre of boundary facets, which can be polygonal in 3D, is reconstructed by interpolating the values at the vertex dofs of each facet using generalised barycentric coordinates. This is achieved following [6] and using power coordinates and the package 2D Triangulation of the geometric library CGAL. We thus write for the boundary facet reconstruction:

$$U_F = \sum_{j \in \mathcal{V}_F} \omega_j U^j, \tag{8}$$

where $\mathcal{V}_F$ is the set of vertices of the facet F, U_F the displacement reconstructed at the barycentre of F and ω_j are the barycentric coordinates. In the case of triangular facets in 3D, Equation (8) reduces to the classical interpolation with barycentric coordinates. In 2D, we can simply use the mid-point interpolation since each boundary facet is a segment.

3.1.3 Gradient reconstruction

The gradient reconstruction from [5, Eq. (2.16)] stems from a discrete Stokes formula. The gradient reconstructed in the cell Ω^i is defined as follows:

$$G_h^i(u_h) := \sum_{F\subset\partial\Omega^i} \frac{|F|}{|\Omega^i|}(U_F - U^i)\otimes n_F = \sum_{F\subset\partial\Omega^i} \frac{|F|}{|\Omega^i|} U_F \otimes n_F, \tag{9}$$

where the summation is over the facets F of Ω^i and n_F is the outward normal to Ω^i on F. The discrete linearised strain in the particle Ω_h^i thus writes:

$$\varepsilon_h^i(u_h) = \frac{1}{2}\left(G_h^i(u_h) + \left(G_h^i(u_h)\right)^T\right). \tag{10}$$

Since strains are reconstructed as piecewise-constants in each cell, the plastic deformation $\varepsilon_{p,h}$ will be taken to be of the same form. Consequently, tensor dofs are placed at each barycentre of each cell Ω^i.

3.2 Space-discrete variational formulation

The discrete unknown is the couple $w_h(t) = (u_h(t), \varepsilon_{p,h}(t)) \in W_h$, evolving in time, where W_h is the space of discrete trial and test functions (up to the handling of Dirichlet boundary conditions). Test functions are written $\tilde{w}_h = (\tilde{u}_h, \tilde{\varepsilon}_{p,h}) \in W_h$. The discretization of Equation (7) is written using these discrete quantities. However, as usual for discontinuous Galerkin methods, the proposed method requires additional penalty terms to ensure the stability of the numerical simulation.

3.2.1 Penalties

The first penalty term takes the form:

$$\sum_{F\in\mathcal{F}^i} \frac{\eta}{h_F}\int_F [u_h]_F \cdot [\tilde{u}_h]_F, \tag{11}$$

where $\mathcal{F}^i$ is the collection of interior facets of the mesh $\mathcal{T}_h$, h_F is the diameter of the facet F, and $[u_h]_F$ is the jump of the values of u_h across F. Writing U^i and U^j the displacements of the two cells sharing F, one has $[u_h]_F := U^i - U^j$. The sign of the jump has no influence on the result. $\eta > 0$ is a user-defined penalty parameter. Equation (11) penalises the jumps of u_h across inner facets. The second penalty term takes inspiration from HHO methods [7] and penalizes jumps between cell values and boundary vertices values:

$$\sum_{F\in\mathcal{F}^b} \frac{\eta}{h_F}\int_F [u_h]_F \cdot [\tilde{u}_h]_F, \tag{12}$$

where $\mathcal{F}^b$ is the collection of boundary facets of the mesh $\mathcal{T}_h$. One has $[u_h]_F = \sum_{i\in\mathcal{V}_F} \omega_i U^i - U^j$, where Ω^j is the cell containing F. The only theoretical requirement on the penalty is that $\eta > 0$. In practice, one might use the lowest value ensuring that the conditioning of the rigidity matrix is satisfactory. The full discrete bilinear form writes:

$$a_h(w_h(t), \tilde{w}_h) := \int_\Omega (\varepsilon_h(u_h)(t) - \varepsilon_{p,h}(t)) : \mathbb{C} : \varepsilon_h(\tilde{u}_h) + \sum_{F\in\mathcal{F}} \frac{\eta}{h_F}\int_F [u_h(t)]_F \cdot [\tilde{u}_h]_F, \tag{13}$$

where $\mathcal{F} = \mathcal{F}^i \cup \mathcal{F}^b$. The associated energy norm is:

$$\|u_h(t)\|_{en}^2 := \|\varepsilon_h(u_h(t))\|_{L^2(\Omega)}^2 + \sum_{F\in\mathcal{F}} \frac{\eta}{h_F} \int_F [u_h(t)]_F^2. \tag{14}$$

3.2.2 Space-discrete variational formuation

The space-discrete formulation writes: Find $w_h = (u_h, \varepsilon_{p,h}) : (0,T) \longrightarrow W_h$ such that a.e. in $(0,T)$ and for all $\tilde{w}_h = (\tilde{u}_h, \tilde{\varepsilon}_{p,h}) \in W_h$:

$$\begin{cases} \displaystyle\int_\Omega \rho \ddot{u}_h(t) \cdot \tilde{u}_h + a_h(w_h(t), \tilde{w}_h) = \int_{\Omega^i} f(t) \cdot \tilde{u}_h + \int_{\partial\Omega_N} g(t) \cdot \tilde{u}_h, \\ \varphi(\Sigma_h^i(t)) \leq 0, \quad \forall \Omega^i, \end{cases} \tag{15}$$

where $\Sigma_h^i(t) = \mathbb{C} : \varepsilon_h^i(u_h(t))$ is the piecewise-constant stress in the cell Ω^i. The coefficients of the space-discrete solution u_h with respect to the piecewise-constant function reconstruction of the dofs are stored in a vector U_h. Assembling the system in a FEM fashion, one gets:

$$\begin{cases} M_h \ddot{U}_h(t) + K_h(\varepsilon_{p,h}(t)) U_h(t) = L_h(t), \\ f(\Sigma_h^i(t)) \leq 0, \quad \forall \Omega^i, \end{cases} \tag{16}$$

where $K_h(\varepsilon_{p,h}(t))$ is the consistent tangent rigidity matrix, M_h the mass matrix, which is naturally diagonal, and $L_h(t)$ the vector of exterior loads. This equation is a system of constrained ODEs that has to be integrated over time. This is done in Section 4.

3.3 Interpretation as a Discrete Element Method

Apart from the dofs at boundary vertices, the method mainly has volumetric dofs which can be interpreted as the displacement of the cell which can be viewed as discrete elements. From Equation (16), one can retrieve the forces exerted on the cells. Moreover, since the mass matrix is diagonal, integrating Equation (16) in time is equivalent to solving the dynamics of each particle individually, the coupling resulting from the rigidity matrix and the constraint.

Let us now give the expression of the corresponding forces in a DEM fashion. Particles are entire cells, for cells with no facet on the boundary, or parts of the cells otherwise, see Figure 1. Indeed, vertices on the boundary are also considered as particles with their associated volume. The Hamiltonian of the system writes:

$$\mathcal{H}_h = \frac{1}{2} V_h^T(t) M_h V_h(t) + \frac{1}{2} U_h^T(t) K_h(\varepsilon_{p,h}(t)) U_h(t) - U_h^T(t) L_h(t). \tag{17}$$

The associated dynamics equations are:

$$\forall i, \begin{cases} \dot{U}_h^i = \dfrac{\partial \mathcal{H}_h}{\partial V_h^i} \\ \dot{V}_h^i = -\left(M_h^i\right)^{-1} \dfrac{\partial \mathcal{H}_h}{\partial U_h^i} \\ \varphi(\Sigma_h^i) \leq 0, \quad \forall \Omega^i, \end{cases}$$

where M_h^i is a 3×3 diagonal matrix with entries m^i. The yield criterion, which is applied in each cell, adds a variational inequality to the system thus giving a constrained Hamiltonian system.

External Forces For a particle Ω^i, the exterior force on the particle is denoted $L_h^i(t) \in \mathbb{R}^d$. L_h^i consists in extracting from $L_h(t) \in \mathbb{R}^{dN}$, where N is the number of particles, the dofs corresponding to the particle Ω^i.

Inertial Forces Similarly, the inertial force on the particle Ω^i writes $m^i \ddot{U}_h^i$ where $m^i = |\Omega^i|\rho$ is the mass of the particle and $\ddot{U}_h^i(t) \in \mathbb{R}^d$ is the acceleration of the particle extracted from $\ddot{U}_h$.

Internal Forces The internal (also called elastic) force applied by the particle Ω^i on the particle Ω^j is written $F_h^{i\to j}$. In Equation (17), the elastic energy has been written using matrices and thus using volume integrals. The elastic energy can also be written "by facet", or as a pair interaction, as follows:

$$\frac{1}{2}\int_\Omega \varepsilon_h(u_h) : \mathbb{C} : \varepsilon_h(u_h) = \sum_{F\in\mathcal{F}} |F| n_F \cdot \frac{1}{2}\left[\Sigma_h\right]_F \cdot U_F = \sum_{\{i,j\}} F_h^{i\to j} \cdot (U_h^i - U_h^j), \tag{18}$$

where the jump $[\cdot]_F$ is consistent with the choice of a normal n_F to the face F. Also, $\{i, j\}$ represents all the particles having a pair interaction (i.e. the value of the dof at x^i is used to reconstruct the value in the cell Ω^j, for instance). Consequently, one has:

$$F_h^{i\to j} = \frac{1}{2}\frac{\partial\left(U_h \cdot K_h(\varepsilon_{p,h}) \cdot U_h\right)}{\partial(U_h^j - U_h^i)}. \tag{19}$$

Remark 3. *As a consequence of Equation (19) and of the symmetry of K_h, the principle of action-reaction with respect to the forces is verified at the discrete level:*

$$F_h^{i\to j} = -F_h^{j\to i}, \quad \forall\{i, j\}.$$

Remark 4. *In a DEM simulation, the computation of the physical behaviour is achieved through the discretization of the internal forces $F_h^{i\to j}$. Thanks to the derivation of these forces from a variational formulation, this method is consistent and can be proved to converge for a Cauchy continuum.*

3.4 Mathematical results

Theorem 5 (Convergence: quasi-static case)**.** *Assuming the solution (u, ε_p) of Equation (7) is such that $u \in C^0\left((0,T); H^2(\Omega)\right)$ and $\varepsilon_p \in L^2((0,T); L^2(\Omega))$, the solution $(u_h(t), \varepsilon_{p,h}(t))$ of Equation (16) converges for a.e. $t \in (0,T)$ towards $(u(t), \varepsilon_p(t))$. One thus has:*

$$\|u_h(t) - u(t)\|_{L^2(\Omega)} + \|G_h(u_h(t)) - \nabla u(t)\|_{L^2(\Omega)} + \|\varepsilon_{p,h}(t) - \varepsilon_p(t)\|_{L^2(\Omega)} \underset{h\to 0}{\longrightarrow} 0, \quad \text{a.e. } t \in (0,T). \tag{20}$$

Moreover, in the purely elastic case, one has the following rate of convergence:

$$\|u_h(t) - u(t)\|_{L^2(\Omega)} + \|G_h(u_h(t)) - \nabla u(t)\|_{L^2(\Omega)} \leq Ch|u(t)|_{H^2(\Omega)}, \quad \text{a.e. } t \in (0,T). \tag{21}$$

3.5 Numerical tests for static and quasi-static evolutions

These numerical tests aim at verifying the correct implementation of the elasto-plastic constitutive laws in our discrete element formulation and the rates of convergence presented above. The piecewise-P^1 reconstruction of displacements $\mathfrak{u}_h : \Omega \longrightarrow \mathbb{R}^d$, which is used for post-processing purposes, is such that:

$$\mathfrak{u}_h(x)|_{\Omega^i} = U_h^i + G_h^i(u_h) \cdot (x - x^i), \quad \forall i. \tag{22}$$

This reconstruction, which is close in spirit to Crouzeix–Raviart finite elements, is nonconforming in $H^1(\Omega; \mathbb{R}^d)$.

Convergence rate elasticity This test case is static. The domain is the unit square with length $L = 1$. Two-dimensional elasticity in weak form is approximated:

$$\int_\Omega \varepsilon(u) : \mathbb{C} : \varepsilon(\tilde{u}) = \int_\Omega f \cdot \tilde{u},$$

where $E = 70 \cdot 10^3 \mathrm{Pa}$ and $\nu = 0.3$. Non-homogeneous Dirichlet boundary conditions are strongly enforced on the entire boundary corresponding to the reference solution which is $u(x, y) = \frac{a}{2}(x^2 + y^2)(e_x + e_y)$ where $a = 0.8$, $f(x, y) = -a(\lambda + 3\mu)(e_x + e_y)$ and (e_x, e_y) is the orthonormal basis attached to the axis of the 2d space. We present the convergence results in Table 1. The results in Table 1

h	$\mathrm{card}(\mathcal{T}_h)$	$\|u - \mathfrak{u}_h\|_{L^2(\Omega)}$	Order	$\|u - u_h\|_{en}$	Order
0.03555	4 464	1.1309e-4	-	1.8561e-2	-
0.01855	17 190	2.8206e-5	2.24	9.0761e-3	1.06
0.00971	68 502	7.1127e-6	1.96	4.6136e-3	1.02
0.00495	271 112	1.7803e-6	2.04	2.2896e-3	1.02

Table 1: Static elasticity convergence: size of the mesh, number of dofs, L^2 error and estimated order of convergence, error in energy norm and estimated order of convergence

show, as expected, that the error in u converges at order 2 in L^2-norm and the error in $\varepsilon(u)$ converges at order 1 in energy norm. Figure 3 exhibits a very close agreement between the norm of the displacement of the computed solution with respect to the reference solution, both computed on a fine mesh.

Swelling of a linearly hardening elasto-plastic cylinder The following test case is quasi-static. It was built using a previous implementation available in [8]. The cited version computed on the finest mesh is used as a reference solution to assert numerical convergence. It is based on a P^2-Lagrange FE solution.

The test case consists in the inner swelling of an infinitely long cylinder. Owing to the symmetries in the problem, the computation is carried out on a quarter of cylinder in 2D in plane strain. A sketch of the problem is presented in Figure 4.

The internal pressure $\mathbf{p}$ is linearly increased from 0 to $p_{\mathrm{lim}} = \frac{2}{\sqrt{3}}\sigma_0 \ln\left(\frac{R_e}{R_i}\right)$, where $\sigma_0 = 250\mathrm{N.m}^{-2}$ is the initial yield stress. A classical Newton–Raphson algorithm is used to solve the equilibrium equations at every loading step. Two curves comparing the presented scheme and the reference implementation are shown in Figure 5 exhibiting a very close agreement. The convergence results are presented in Table

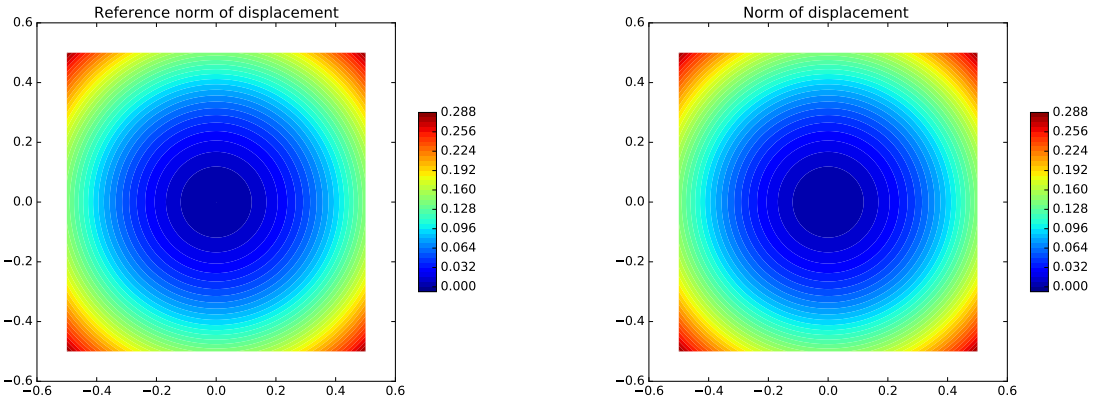

Figure 3: Norm of the displacement in the square domain. Left: Reference solution computed on a fine mesh. Right: present solution computed on a fine mesh.

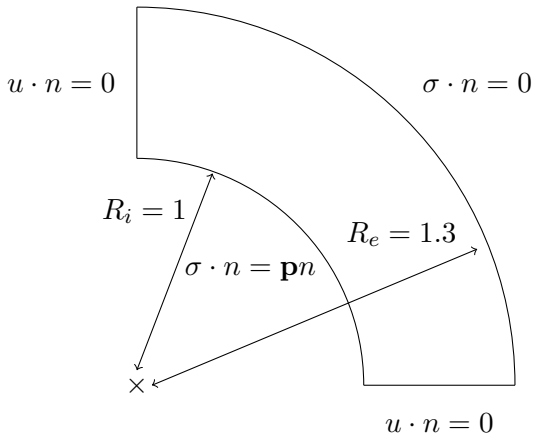

Figure 4: Sketch of the swelling of the cylinder

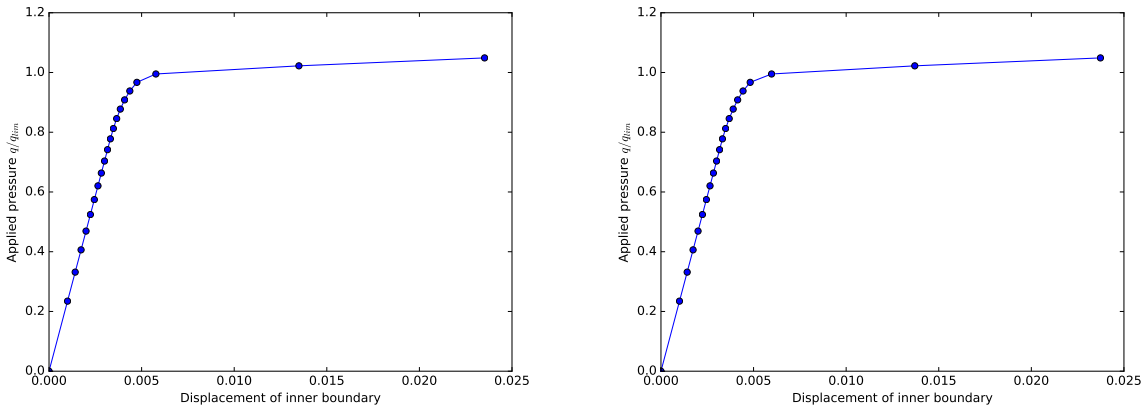

Figure 5: Swelling of the cylinder. Left: Reference solution computed on a fine mesh. Right: present solution computed on a fine mesh.

2. The errors in L^2 and energy norm are the maximal error over the 20 time-steps. The results in Table

h	$\mathrm{card}(\mathcal{T}_h)$	$\|u - \mathfrak{u}_h\|_{L^2(\Omega)}$	Order	$\|p - p_h\|_{L^2(\Omega)}$	Order
0.07735	992	2.2128e-4	-	2.2037e-03	-
0.04217	3 412	6.2420e-5	2.05	1.1315e-03	1.08
0.02879	7 588	1.7331e-5	2.50	6.4657e-04	1.21
0.02172	13 380	1.0784e-5	2.32	4.8786e-04	1.16
0.01464	29 528	4.2459e-6	2.33	2.9605e-04	1.18

Table 2: Swelling of a linearly hardening elasto-plastic cylinder: Size of mesh, Number of dofs, L^2 error in u and estimated order of convergence, L^2 error in p and estimated order of convergence

2 show that the method converges at order 2 in the reconstructed displacement $\mathfrak{u}_h$ and at order 1 in the cumulated plastic strain p_h in L^2-norm. It also converges at order 1 in the H^1-norm.

4 Space-Time discretization

The space-discretization reduces through Equation (16) to a system of ODEs, which has to be integrated in time. The computations are performed using an explicit Störmer–Verlet time-integration.

4.1 Time discretization

The time interval $[0, T]$ is discretised as $0 < t_1 < ... < t_n < t_{n+1} < ... < T$ using a constant time-step Δt which respects the following CFL stability condition:

$$\Delta t \ < \ 2\sqrt{\frac{m}{\Lambda}}, \tag{23}$$

where m is the smallest component of the diagonal mass matrix M_h and Λ the largest eigenvalue of the rigidity matrix $K_h(\varepsilon_{p,h} = 0)$. Using a constant time-step satisfying Equation (23) will be enough as plasticity does not increase the rigidity of the system.

Remark 6 (CFL condition)**.** *As stated in Section 3.1, interpolation is preferred to extrapolation for the facet reconstructions when one intends to undertake dynamics computations with an explicit integrator. Indeed, when extrapolating, the barycentric coordinates do not take values in the interval* $(0, 1)$*. The barycentric weights can increase the eigenvalues of the rigidity matrix and thus deteriorate the CFL condition.*

The values at the discrete times U_h^n approximate the time-continuous values $U_h(t_n)$. The displacements U_h^n are calculated at every time-step, whereas the velocities $\dot{U}_h^{n+1/2}$ are approximated at the half time-steps $t_{n+1/2} = \frac{t_n + t_{n+1}}{2}$. Velocities are still written with an upper dot even if they are no longer derivatives. Displacements are then computed as:

$$U_h^{n+1} = U_h^n + \dot{U}_h^{n+1/2} \cdot (t_{n+1} - t_n). \tag{24}$$

Strains and stresses are computed at t^{n+1}. We then check whether the yield criterion is verified. An explicit return mapping algorithm is used to update the plastic variables if necessary. Stresses are recomputed if plastic flow has occurred. Finally, forces are computed at each time-step as:

$$F_h^{n+1} := K_h(\varepsilon_{p,h}^{n+1}) \cdot U_h^{n+1} - L_h^{n+1}. \tag{25}$$

Velocities are then updated as

$$\dot{U}_h^{n+3/2} = \dot{U}_h^{n+1/2} + M_h^{-1} F_h^{n+1} \Delta t. \tag{26}$$

Finally, initial conditions are discretised as

$$\begin{cases} U_h^0 = \mathcal{I}_h u_0 \\ \dot{U}_h^{1/2} = \mathcal{I}_h v_0 \end{cases} \tag{27}$$

where $\mathcal{I}_h$ is the interpolation consisting in taking the value of a continuous function at every dof position.

4.2 Mathematical results

Theorem 7 (Convergence: dynamic case)**.** *Assuming the solution (u, ε_p) of Equation (7) is such that $u \in C^0\left((0,T); H^2(\Omega)\right)$ and $\varepsilon_p \in C^0((0,T); L^2(\Omega))$, the discrete solution $\left(u_h^n, \varepsilon_{p,h}^n\right)_n$ converges, when $\Delta t \to 0$ and $h \to 0$, towards (u, ε_p) the solution of Equation (7).*

$$\max_n \|u_h^n - u(t^n)\|_{L^2(\Omega)} + \left(\sum_n \Delta t \|G_h\left(u_h^n\right) - \nabla u(t^n)\|_{L^2(\Omega)}^2 \right)^{1/2} + \max_n \|\varepsilon_{p,h}^n - \varepsilon_p(t^n)\|_{L^2(\Omega)} \longrightarrow 0, \tag{28}$$

Moreover, in the purely elastic case, one has the following rates of convergence:

$$\max_n \|u_h^n - u(t^n)\|_{L^2(\Omega)} + \left(\sum_n \Delta t \|G_h(u_h^n) - \nabla u(t^n)\|_{L^2(\Omega)}^2 \right)^{1/2} \leq C(h + \Delta t^2). \tag{29}$$

4.3 Numerical test

The reference solution for this test case is an implementation available in [8]. This test case consists in computing the oscillations of a beam with rectangular section, clamped at one end and loaded by a uniform vertical traction at the other end. A uniform boundary stress $g(t)$ of value -1 is applied in the x direction on the loaded surface for $0 \leq t \leq \frac{T}{5}$. Figure 6 shows a sketch of the dynamic experiment.

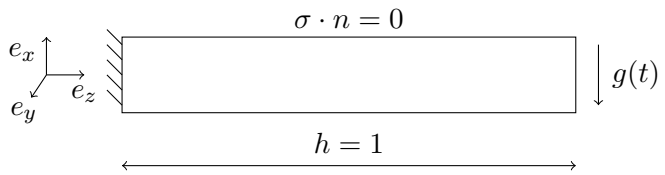

Figure 6: Sketch of the dynamics experiment

The computation is performed in 3D. The reference solution is computed using P^1-Lagrange finite elements and a Störmer–Verlet time-integration. The displacement and velocity at the loaded tip of the beam, computed with the proposed method which is also coupled to an explicit Störmer–Verlet time-integration, are compared to the reference solution in Figure 7. The rather fine mesh is the same for the two computations.

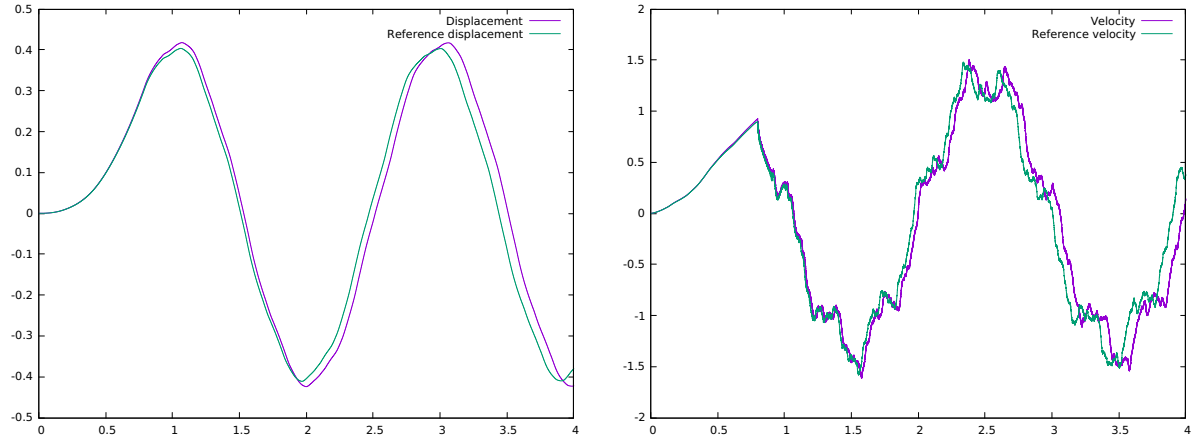

Figure 7: Comparison between the proposed scheme and the reference solution. Left: Displacement at the loaded tip of the beam. Right: Velocity at the same point.

The agreement between the computed and reference solution in Figure fig:comparaison dynamique 1 is quite satisfying.

5 Conclusion

We have presented a new Discrete Element Method which is a consistent discretization of a Cauchy continuum and which only requires continuum macroscopic parameters like Young's modulus and Poisson's ratio. We have presented the reconstruction of strains for a piecewise-constant reconstruction of displacements and plastic strains. Finally, we have shown on various examples that the present scheme converges for hardening elasto-plastic materials and that, under appropriate regularity hypotheses, the scheme is second-order convergent in space in the L^2-norm and first-order convergent in the energy norm.

Future work includes adapting the present framework to dynamic cracking computations and contact. With a view towards fragmentation computation, stabilization techniques for shocks are under study. Future work also includes using an adaptation of the present scheme to compute Cosserat continua.

References

[1] L. Monasse, C. Mariotti, An energy-preserving Discrete Element Method for elastodynamics, ESAIM: Mathematical Modelling and Numerical Analysis, 46 (2012) 1527–1553.

[2] J. Droniou, R. Eymard, T. Gallouët, C. Guichard, R. Herbin, The gradient discretisation method, Springer, 2018.

[3] M. Jebahi, D. André, I. Terreros, I. Iordanoff, Discrete element method to model 3D continuous materials, John Wiley & Sons, 2015.

[4] D. A. Di Pietro, Cell centered Galerkin methods for diffusive problems, ESAIM: Mathematical Modelling and Numerical Analysis, 46 (2012) 111–144.

[5] R. Eymard, T. Gallouët, R. Herbin, Discretization of heterogeneous and anisotropic diffusion problems on general nonconforming meshes SUSHI: a scheme using stabilization and hybrid interfaces, IMA Journal of Numerical Analysis, 30 (2009) 1009–1043.

[6] M. Budninskiy, B. Liu, Y. Tong, M. Desbrun, Power coordinates: a geometric construction of barycentric coordinates on convex polytopes, ACM Transactions on Graphics (TOG), 35 (2016) 241.

[7] D. A. Di Pietro, A. Ern, A hybrid high-order locking-free method for linear elasticity on general meshes, Computer Methods in Applied Mechanics and Engineering, 283 (2015) 1–21.

[8] J. Bleyer, Numerical Tours of Computational Mechanics with FEniCS, 10.5281/zenodo.1287832, 2018.